ACS APPLIED MATERIALS & INTERFACES

Research Article

www.acsami.org

Photocatalytic Activity of $ZnWO_4$: Band Structure, Morphology and Surface Modification

Cuiling Zhang,[†,‡] Hulin Zhang,[†] Kaiyou Zhang,[†] Xiaoyan Li,[†] Qiang Leng,[†] and Chenguo Hu*[,†]

[†]Department of Applied Physics, Chongqing University, Chongqing 400044, People's Republic of China

[‡]School of Computer Science and Information Engineering, Chongqing Technology and Business University, Chongqing 400067, People's Republic of China

ABSTRACT: Photocatalytic degradation of organic contaminants is an important application area in solar energy utilization. To improve material photocatalytic properties, understanding their photocatalytic mechanism is indispensable. Here, the photocatalytic performance of $ZnWO_4$ nanocrystals was systematicly investigated by the photodegradation of tetraethylated rhodamine (RhB) under simulated sunlight irradiation, including the influence of morphology, AgO/$ZnWO_4$ heterojunction and comparison with $CoWO_4$ nanowires. The results show that the photocatalytic activity of $ZnWO_4$ is higher than that of $CoWO_4$, and the $ZnWO_4$ nanorods exhibit better photocatalytic activity than that of $ZnWO_4$ nanowires. In addition, the mechanism for the difference of the photocatalytic activity was also investigated by comparison of their photoluminescence and photocurrents. AgO nanoparticles were assembled uniformly on the surface of $ZnWO_4$ nanowires to form a heterojunction that exhibited enhanced photocatalytic activity under irradiation at the initial stage. We found that a good photocatalyst should not only have an active structure for electrons directly to transfer from the valence band to the conduction band without the help of phonons but also a special electronic configuration for the high mobility, to ensure more excited electrons and holes in a catalytic reaction.

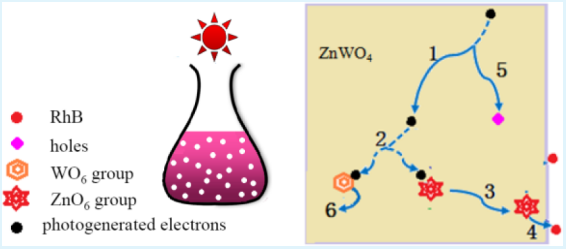

KEYWORDS: *nanomaterials, heterostructure, photocatalytic activity, band structure, carrier transport*

INTRODUCTION

To effectively utilize solar light and reduce environmental pollution, exploration of photocatalysis of materials is interesting and challenging work. Photocatalysts, such as TiO_2 and ZnO,[1−10] have been studied in the past several decades. Results of those studies have suggested that broader light absorption range and higher electron mobility contribute to the high photocatalytic activity. In addition, crystal structure, specific surface area, particle size, number of defective sites and electron−hole recombination rate are important in the development of highly active photocatalysts for solving environmental pollution problems. To obtain visible-light-driven catalytic activity, new photocatalysts (such as WO_3, Bi_2WO_6, $NdVO_4$),[11−13] doped photocatalysts (such as Sn^{2+}, Ni, Fe)[14,15,7] and surface modification have been developed.[16−19]

Tungstates have caught the attention of researchers as photocatalysts since tungsten oxide ($PbWO_4$) was found capable of photocatalytically splitting H_2O into H_2 and O_2.[20] Conventionally, tungtsates have sufficient chemical stability, but few reports are available about their active photocatalysts except for $CdWO_4$, $ZnWO_4$ and Bi_2WO_6.[21−23] Most of the tungsten metal oxides are found to be photocatalytically inactive for the photodegradation of an organic contaminant. Meanwhile, several recent studies indicate that a series of metal oxides with the d^{10} and d^0 electronic configurations have been determined to be more photocatalytically active under UV irradiation for larger electron transport, especially in octahedral MO_6 unit transition metal ions.[24] $ZnWO_4$, a wolframite tungsten metal oxides with $d^{10}s^2$-d^0 electronic configuration,[25] has been investigated for water splitting and mineralization of organic pollutants under UV irradiation in recent years.[21,22] Literature shows that the photocatalytic activity of $ZnWO_4$ is a little higher than that of P-25 (Degussa) in gaseous[26] and other tungstates $M^{II}WO_4$ (M = Co^{II}, Ni^{II}, Cu^{II}, Pb, Cd and Ca),[21,27] and Bi_2WO_6 under UV irradiation.[28] That is to say, the environment-friendly $ZnWO_4$ has good photocatalytic performance under UV irradiation.

However, $ZnWO_4$ displayed relatively poor photoactivity under visible light in comparison to that of Bi_2WO_6 for its narrow spectral scope.[21,28,29] The improvement of photocatalytic activity of $ZnWO_4$ is hampered by its large energy band gap and fast recombination of photogenerated electron−hole pairs. To improve the photocatalytic activity of $ZnWO_4$, three strategies have been adopted to improve its activity as a photocatalyst. One is to increase the specific surface area of $ZnWO_4$ catalyst via controllable morphology.[30] The second is to extend the photoresponse region by the doping of nonmetals or transition metals[31] and the third is to minimize the recombination of electron and hole by effective separation of the photogenerated electron−hole pairs and the fast interfacial

Received: June 11, 2014
Accepted: August 7, 2014
Published: August 14, 2014

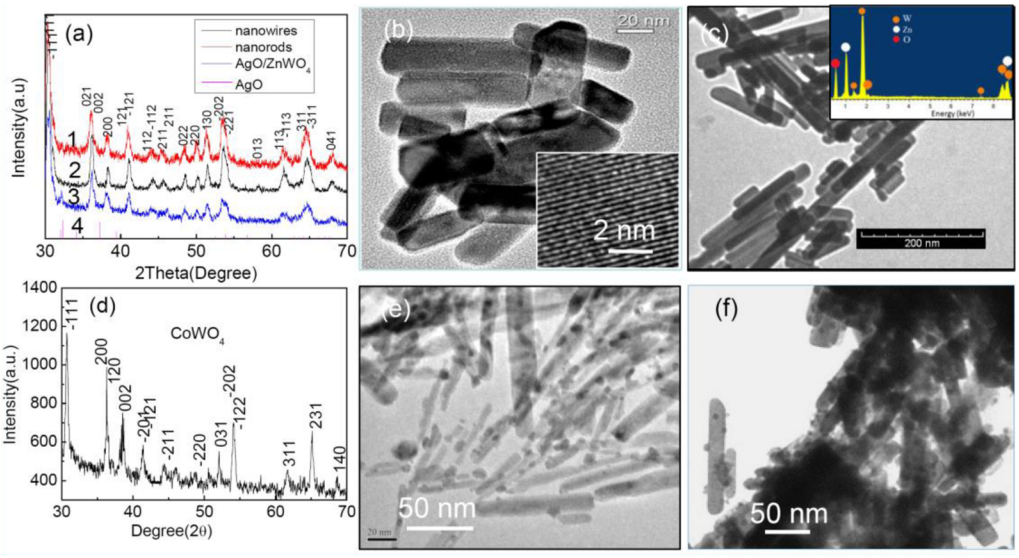

Figure 1. X-ray diffraction (XRD) patterns (a) of the $ZnWO_4$ nanorods (1), nanowires (2), $AgO/ZnWO_4$ (3); scanning electron microscopy (SEM) (b) and high resolution (HR)TEM (inset b) images of the $ZnWO_4$ nanorods; SEM image (c) and EDS (inset c) of the $ZnWO_4$ nanowires; XRD pattern (d) and SEM image (e) of the $CoWO_4$ nanowires; SEM image of the $AgO/ZnWO_4$ heterojunction (f).

charge transfer to the electron donor/electron acceptor, and more electrons and holes participates in photocatalytic reactions.[18,32] Photocatalytic activity of $ZnWO_4$ is promoted by the increase in aspect ratio of the $ZnWO_4$ nanorods.[33] The photocatalytic activity of the $ZnWO_4$ with doping fluorine nanoparticles annealed at 450 °C for 1 h and chlorine (R_{Cl} = 0.3) can be enhanced about 50%[26] and approximately 4 times,[34] respectively. BSA−$ZnWO_4$ (BSA = bovine serum albumin) shows superior degradation efficiency and reusability to $ZnWO_4$ for MB degradation.[35] The g-C_3N_4−$ZnWO_4$ composite heterojunctions show higher photocatalytic activity than the pure g-C_3N_4 or $ZnWO_4$ under visible-light irradiation and an 80% increase under ultraviolet−visible-light irradiation.[36] Therefore, the investigation concerning the relationship between photocatalytic activity and different tungsten metal oxides, the aspect ratio of one-dimensional nanostructured crystals and surface modification is quite meaningful.

Photocatalysts modified by loading of noble metal particles or some metal oxides, such as platinum, gold, palladium, silver,[8,16,17] Ag_2O[10,18] and AgO,[19] presents high photocatalytic activity. Aysin suggested that Ag was loaded on TiO_2 powders in the form of AgO.[37] It well-known that Ag_2O is unstable under visible-light irradiation and decomposes into metallic Ag during the photocatalytic decomposition of organic substances.[38] However, after partial in situ formation of Ag on the surface of Ag_2O, the Ag_2O/Ag composite can work as a stable and efficient visible-light photocatalyst.[38] But some metal oxides modified photocatalysts (such as Ag_2O/TiO_2) have bad cyclic stability under UV light irradiation because Ag_2O yields Ag clusters.[18] In general, noble metal oxides loading on photocatalysts can improve their photocatalytic activities and the role of a metal cluster on photocatalysts modified by metal oxides is interesting. The AgO-loaded $ZnWO_4$ photocatalyst for degradation of tetraethylated rhodamine (RhB) under simulated solar light has not been studied.

In the present work, to know the key point that affects photocatalytic performance, the photocatalytic activity of $ZnWO_4$ with $d^{10}s^2$-d^0 configuration and $CoWO_4$ with $d^7s^2d^0$ configuration is compared from the viewpoint of electronic structures. Different morphology $ZnWO_4$ nanorods and nanowires are synthesized by hydrothermal method with different pH and concentration of reactants, respectively. $AgO/ZnWO_4$ heterojunctions are prepared by a chemical precipitation method under UV irradiation. The mechanisms of band structure, surface modification and morphology on the photocatalytic activity of $ZnWO_4$ are discussed in detail.

EXPERIMENTAL SECTION

$ZnWO_4$ was prepared by a hydrothermal method. For the synthesis of $ZnWO_4$ nanorods, typically, 4 mmol $ZnCl_2{\cdot}6H_2O$ and 4 mmol $Na_2WO_4{\cdot}2H_2O$ were put into a 25 mL autoclave vessel with 20 mL of deionized water and heated to 180 °C for 24 h. For the synthesis of $ZnWO_4$ nanowires, 2 mmol $ZnCl_2{\cdot}6H_2O$ and 2 mmol $Na_2WO_4{\cdot}2H_2O$ were put into a 25 mL autoclave vessel with 20 mL pH = 10 deionized water and heated at 180 °C for 24 h. The white precipitate was washed with deionized water for several times and dried at 60 °C for 1 h. $CoWO_4$ nanowires were prepared by solvothermal method. 0.1 M $CoCl_2{\cdot}6H_2O$ and 0.1 M $Na_2WO_4{\cdot}2H_2O$ were placed into a Teflon vessel with 16 mL of absolute ethanol and 4 mL of ammonia (pH = 10). The vessel was heated to 180 °C for 24 h in a furnace. After the vessel cooled to room temperature, the blue solid product $CoWO_4$ was collected, washed several times with deionized water and ethanol and dried at 60 °C for 1 h. The AgO-$ZnWO_4$ heterostructure was obtained by a chemical precipitation method under UV irradiation. Typically, 25 mL of 0.1 mol/L $AgNO_3$, 25 mL of 0.5 mol/L glucose and 0.1 g $ZnWO_4$ nanowires were mixed and vigorously stirred for 4 h under ultraviolet irradiation. Finally, about 0.8 g of sample was obtained by a washing with deionized water and ethanol and centrifugation process and dried at 60 °C for 1 h. The same process also takes place with the samples of AgO−$ZnWO_4$ after photodegradation.

Characterization. Transmission electron microscopy (TEM, JEOL-4000EX) was used to characterize the morphology and size of the synthesized samples. The crystal phase and chemical composition were characterized by an X-ray diffractometer (BDX3200) equipped with Cu Kα radiation (λ= 1.5418 Å) at a scanning speed of 2° per minute in the 2θ range from 20° to 80°. Electronic properties of the tungstates were studied on an ESCALab MKII X-ray photoelectron spectrometer, using nonmonochromatized Mg Kα X-ray as the excitation source. The specific surface areas were calculated by a multipoint Brunauer−Emmett−Teller (BET) analysis of the nitrogen adsorption isotherms recorded on a surface area analyzer (Micromeritics ASAP 2020 M).

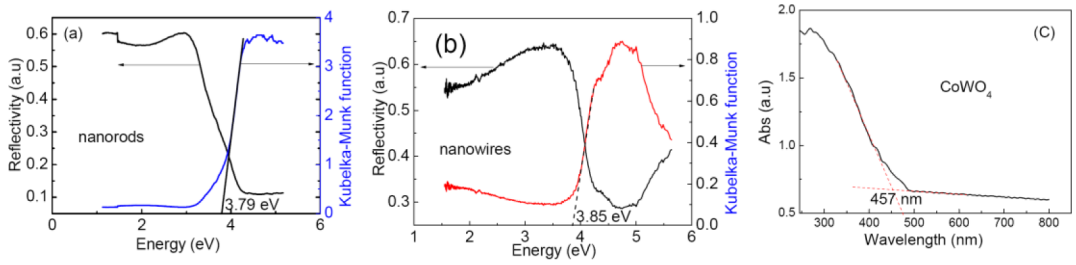

Figure 2. UV−visible reflection spectrum and Kubelka−Munk function of the $ZnWO_4$ nanorods (a) and nanowires (b); the absorption spectrum of the $CoWO_4$ (c).

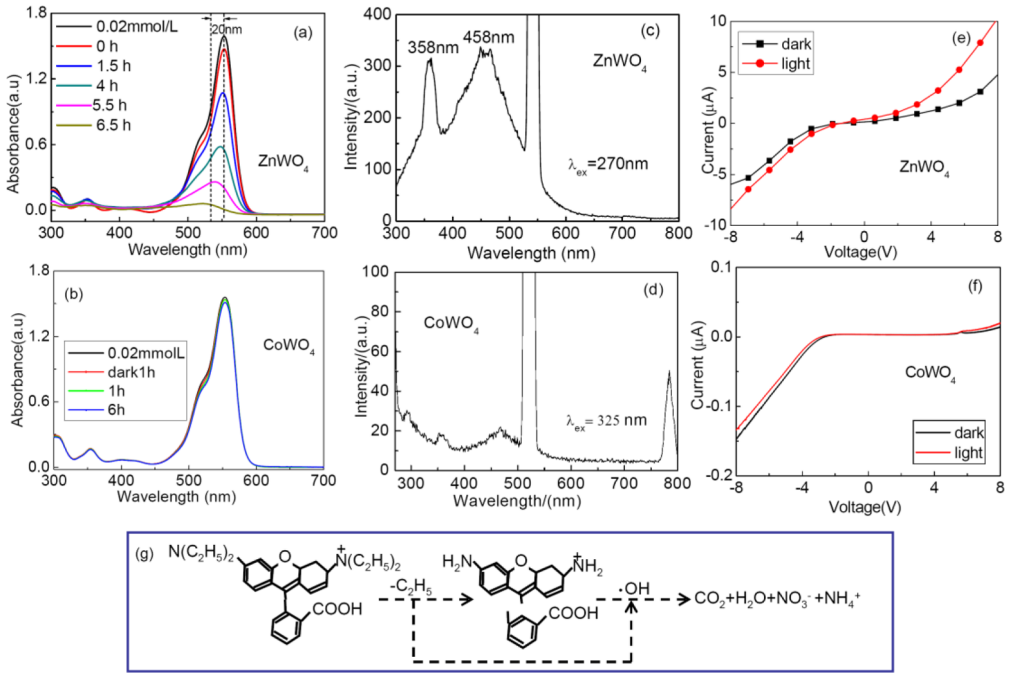

Figure 3. Absorption spectrum of RhB dye solution with the $ZnWO_4$ nanorods (a) $CoWO_4$ (b) in different stages under illumination of the simulated sunlight; the room-temperature emission spectrum of $ZnWO_4$ nanowires (c) and $CoWO_4$ nanowires (d) at the excitation wavelength 270 and 325 nm, respectively; the photocurrent and dark current of $ZnWO_4$ (e) and $CoWO_4$ (f); the degradation process of RhB (g).

Optical Property Measurement. To examine the optical band gap of the samples, we measured the reflectance spectrum of a film made of the $ZnWO_4$ nanorods and nanowires on a quartz slice by UV−vis-NIR spectrophotometer (UV 3600) under a normal incidence of light. The absorption spectra of $CoWO_4$ nanowires and AgO−$ZnWO_4$ after photodegradation were also measured. A photoelectric device was fabricated with three facile steps to investigate the photosensitive properties of the obtained $ZnWO_4$ and $CoWO_4$ nanostructures. The first step is to obtain a nanostructure film by pressing tungstates under the pressure of 10 MPa. The second step is to clean two pieces of conductive glasses (FTO) ultrasonically with a detergent solution and deionized water several times. The last step is to fabricate a photodetector device by encapsulating the sandwich structure with epoxy resin. The photoelectronic performance of the device was investigated under the irradiation of simulated sunlight (CHF-XM-500W), and the photocurrent was recorded using a computerized data acquisition system equipped with a source meter (KEITHLEY 2400).

Photocatalytic Degradation. 100 mL of an aqueous suspension of RhB (1×10^{-5} and 2×10^{-5} mol/L, respectively) and certain amounts of samples (30 and 100 mg) were placed in a 100 mL beaker. The suspensions were magnetically stirred in the dark for 30 min to establish the adsorption/desorption equilibrium at 15 °C before illumination. A simulated sunlight instrument (CHF-XM-500W) with a power of 100 mW/cm^2 was used as the illumination source. The residual RhB concentration was detected using UV-3600.

RESULTS AND DISCUSSION

XRD patterns in Figure 1a indicate high crystallization of the $ZnWO_4$ samples. All diffraction peaks are readily indexed to a pure monoclinic wolframite-type monoclinic phase (P2/a (13)) of $ZnWO_4$ (JCPDS card No. 15-0774). The peak intensity of $ZnWO_4$ nanowires (2) is slightly stronger than that of the $ZnWO_4$ nanorods (1), which indicate a better crystallization. The XRD pattern (3) demonstrates that the $ZnWO_4$ surface is modified by AgO. Compared with $ZnWO_4$ nanowires, the position of $ZnWO_4$ peaks does not change and the relative height of $ZnWO_4$ peaks reduces because of the coverage by AgO. The extra weak peak of $ZnWO_4$ nanowires appears at 32.18°, which may be the superposition of peaks AgO (JCPDS card No. 22-0472) (200) and (−111)). The two peaks are too close and small to tell because of the small size of the AgO particles. The TEM image in Figure 1b exhibits the homogeneous morphology of the $ZnWO_4$ with short nanorods of 60−100 nm in length and 20 nm in width. The HRTEM image in the inset of Figure 1b demonstrates single-crystal structure of the nanorods. Figure 1c shows that the nanowire-like morphology of the $ZnWO_4$ crystallites about 200 nm in length and 20 nm in width. The energy dispersive X-ray spectroscopy (EDS) spectrum in the inset in Figure 1c shows

that the corresponding sample is composed of Zn, W and O with an atom ratio of Zn, W and O close to 1:1:4. The XRD pattern of $CoWO_4$ presented in Figure 1d agrees well with JCPDS Card No. 15-0867 and is a wolframite-type monoclinic phase. The TEM image in Figure 1e shows the $CoWO_4$ nanwires is about 20 nm in width and 200 nm in length. Therefore, the zinc tungstates and cobalt tungstates have large specific surface areas and high aspect ratios. Figure 1f shows the TEM image of AgO loaded $ZnWO_4$ nanowires. Some small particles, about 5 nm, can be clearly observed on the surface of the $ZnWO_4$ nanowires, indicating that AgO nanoparticles are dispersed on the surface of the $ZnWO_4$ nanowires.

The optical energy gap (E_g) of the samples can be obtained from Kubelka–Munk (K-M) function, which can be expressed by the following[39]

$$\alpha = S(1 - R)^2/2R \quad (1)$$

where α, R and S are absorbance, reflectivity and scattering factor, respectively. S can be taken as a constant because an ideal diffuse reflection can be assumed when the size of individual nanowires is much less than the thickness (about 1 mm) of the nanomaterial film. The K-M function of the $ZnWO_4$ nanorods and $ZnWO_4$ nanowires can be plotted vs photon energy, as is shown in Figure 2a,b. There is one linear part of the curve in the K-M function, from which the optical band gap calculated by extrapolation of linear part of the curve to zero, that is, E_g = 3.79 eV for $ZnWO_4$ nanorods and E_g = 3.85 eV for $ZnWO_4$ nanowires, which is similar to the previous report of 3.8–5.7 eV.[25] The optical band gap of $CoWO_4$ is E_g = 2.7 eV as is shown in Figure 2c, which agrees with the previous report.[25] So, the $ZnWO_4$ absorption region of sunlight is narrower than that of $CoWO_4$ and only less than 3% and about 25% sunlight can be utilized by $ZnWO_4$ and $CoWO_4$, respectively.

As a widely used dye, tetraethylated rhodamine (RhB) is selected as a pollutant to evaluate the photocatalytic efficiency of the as-prepared tungstate catalysts. It is well-known that semiconductors under illumination with a photon energy larger than their band gap can produce electron–hole pairs. Some of the photogenerated electrons and holes transferring to the surface of the crystal can react with H_2O and molecular oxygen O_2 to produce reactive species ·OH (hydroxyl radical), which is a strong oxidizing agent, to degrade the organic dye into small molecules like CO_2, H_2O, etc.[40,41] A gradual decrease in RhB absorption under photocatalytic degradation can be observed in the absorption spectra of an RhB aqueous solution. Figure 3a,b shows temporal evolution of the absorption spectra of an RhB aqueous solution (2×10^{-5} mol·L^{-1}) in the presence of the 30 mg of $ZnWO_4$ nanorods or $CoWO_4$ nanowires under simulated sunlight irradiation, respectively. The characteristic peaks of RhB change both in the strength and position compared with the starting materials. The absorption peak shown in Figure 3a decreases and moves to shorter wavelengths. The color of the dye solution changes from its initial deep red to a light red, and then to transparent, which can be observed by naked eyes. Meanwhile, the absorption for ultraviolet also decreases until no absorption is found.

Generally, the mechanism of the photocatalytic reaction of RhB involved the de-ethylation and the cleavage of conjugated chromophore structure, which can be characterized by the shift of the maximum absorption band and by the change in the absorption maximum of RhB, respectively. Usually, these two reactions take place simultaneously and competitively in the photocatalysis process. Because the wavelength of absorption peak shifts 17 nm for $ZnWO_4$ nanorods, and a change in the absorption maximum can be observed, the two reactions might take place simultaneously in the photocatalytic processes. But it is dominated by de-ethylation. The absorption maximum at about 300–400 nm changes slowly, which indicates that there are small molecules or molecular fragment (such as CO_2^-) in the photocatalytic reaction. A possible photocatalytic reaction of the $ZnWO_4$ nanorods system is proposed as follows:

$$ZnWO_4 \xrightarrow{h\nu} ZnWO_4(h^+) + ZnWO_4(e^-) \quad (2)$$

$$e^- + O_2 + H_2O \rightarrow \cdot HO + OH^- \quad (3)$$

$$h^+ + 2H_2O \rightarrow \cdot HO + H^+ \quad (4)$$

$$OH^- + h^+ \rightarrow \cdot OH \quad (5)$$

$$\cdot OH + O_2 + RhB \rightarrow CO_2 + H_2O + NO_3^- + NH_4^+ \quad (6)$$

Figure 3g indicates the process of de-ethylation for RhB, and then the de-ethylation and partial de-ethylation of RhB are constantly split through cleavage of the conjugated chromophore structure by ·HO oxidation.

Compared with the active photocatalyst $ZnWO_4$, photocatalytic degradation of RhB aqueous solution with $CoWO_4$ nanowires has no obvious effect in 6 h, indicating the much weaker degradation ability of $CoWO_4$ than that of $ZnWO_4$. The results are consistent with the previous studies.[21] In terms of the band gap, the $CoWO_4$ nanowires could absorb more solar energy and generate considerable photoinduced carriers, and should have better photocatalytic ability. Therefore, there should be other causes for the difference of photocatalysis other than the band gap.

As an important luminescence material, the recombination luminescence of tungstates in the recombination center would reduce photoinduced carriers and degradation efficiency. Both the ZnO_6 and CoO_6 groups in $ZnWO_4$ and $CoWO_4$ also have a strong ability to capture photoinduced carriers. Meanwhile, there is competition of capturing photoinduced carriers between WO_6 and ZnO_6 or CoO_6. Therefore, the investigation of the electric transfer and trapping of photoinduced carrier in $ZnWO_4$ nanorods and $CoWO_4$ nanowires is presented in Figure 3. The $ZnWO_4$ nanorods show a strong PL emission peak at 358 nm and a wide peak centered at 458 nm (Figure 3c). The PL emission of the $CoWO_4$ almost quenches in the visible range at room temperature (Figure 3d). So, the WO_6 group has a stronger carrier capture ability and the electrons are mainly captured by the WO_6 group in $ZnWO_4$. However, the weak PL of $CoWO_4$ indicates that the electrons are rarely captured by WO_6 in $CoWO_4$. Figure 3e,f reveals that the photocurrent is twice the dark current in the $ZnWO_4$ device, while the photocurrent and dark current are the same in the $CoWO_4$ device. This means that there are more photoproduced carriers in $ZnWO_4$ than in $CoWO_4$ and the mobility of the photoproduced carriers in $ZnWO_4$ is higher than that in $CoWO_4$. It seems that the capture and recombination of photogenerated electrons and holes in $CoWO_4$ occur mainly in the CoO_6 group for the weak PL and photocurrent.

To understand the carrier's capture and transport of $ZnWO_4$ and $CoWO_4$ on photodegradation efficiency, we calculated their band structures based on density functional theory (DFT). All the calculations and the Brillouin zone integration

were performed with W $5s^2$ $5p^6$ $5d^4$ $6s^2$, Zn $3d^{10}$ $4s^2$, Co $3d^7$ $4s^2$ and O $2s^2$ $2p^6$ treated as valence electrons. In Figure 4a, we can see that the band structure of $ZnWO_4$ is direct because the top of the valence band and the bottom of the conduction band locate at the same Y point, which is different from $CoWO_4$ (Figure 4b), indicating that $ZnWO_4$ may be a good optical material for the better light absorption. Such results are consistent with the above experiments that the electron transition of $ZnWO_4$ nanorods from the valence band to the conduction band has one absorption peak. The calculated band gap is 2.9 and 0.8 eV for $ZnWO_4$ and $CoWO_4$, which is underestimated in comparison with the experimental values of 3.8 and 2.7 eV due to the limitations of GGA.

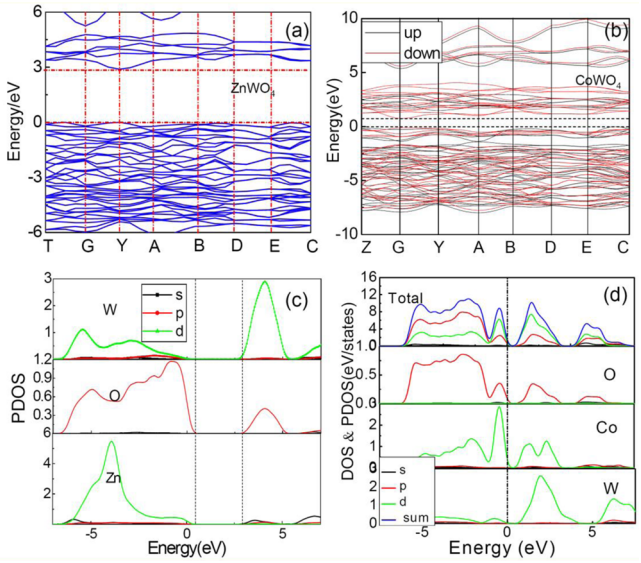

Figure 4. Band structure of $ZnWO_4$ nanocrystal (a) and $CoWO_4$ nanocrystal (b); the PDOS of $ZnWO_4$ (c) and the total DOS and PDOS of $CoWO_4$ nanocrystal (d).

The PDOS of $ZnWO_4$ in Figure 4c shows that the top valence band associates with O 2p, W 5d and Zn 3d, among which the main contribution is O 2p. The conduction is composed of O 2p, W 5d and Zn 4s, among which the W 5d contributes mainly. And although there is competition between the ZnO_6 and WO_6 groups in the carrier's capture, photo-induced carriers mainly concentrate on the WO_6 group. The length of coordination O atoms to W is 0.207 132, 0.208 725 and 0.229 238 nm, indicating that octahedron of WO_6 is distorted, which results in the Jahn–Teller Effect. According to ligand field theory, the energy of WO_6 octahedron will split into ground state $^1A_{1g}$ and excited states $^3T_{1g}$, $^1T_{1g}$, $^3T_{1u}$, $^1T_{1u}$, in which the transition from $^1A_{1g}$ to $^1T_{1u}$ are allowed and the transition from $^1A_{1g}$ to $^3T_{1g}$, $^1T_{1g}$, $^3T_{1u}$ are forbidden while they are partially allowed due to the Jahn–Teller Effect. When under irradiation the electron majority jumps from ground states $^1A_{1g}$ to $^1T_{1u}$ and some electrons jump to the excited states $^3T_{1g}$, $^1T_{1g}$ and $^3T_{1u}$. So, the great majority of electrons in excited states will mainly be captured by WO_6 and then join through radiative or nonradiative recombination with holes in the WO_6 group. Because of the competition on electron capture between WO_6 and ZnO_6, some excited electrons can be captured by ZnO_6 and transfer easily for the cruise features in Zn 4s states, which contribute to the effective electron–hole separation. In the process, effective optoelectronic transfer to the interface is the key point for photocatalysis.

However, the PDOS of $CoWO_4$ in Figure 4d shows that the top valence band associates with O 2p, W 5d and Co 3d, among which the main contribution is from Co 3d, and the conduction is mainly composed of O 2p, W 5d and Co 3d, among which the Co 3d contributes mainly. But the CoO_6 group plays the same role as WO_6 in $ZnWO_4$ for the localization. The effective electronic and hole's transmission are weak in the conductive band and valence band, respectively. Few electrons of Co^{2+} in valence band are excited to conductor band by light and captured by W 5d in conductive band with the help of phonon, and majority excited electrons are captured in the inactivation center (Co) and transfers energy to host lattices in the form of

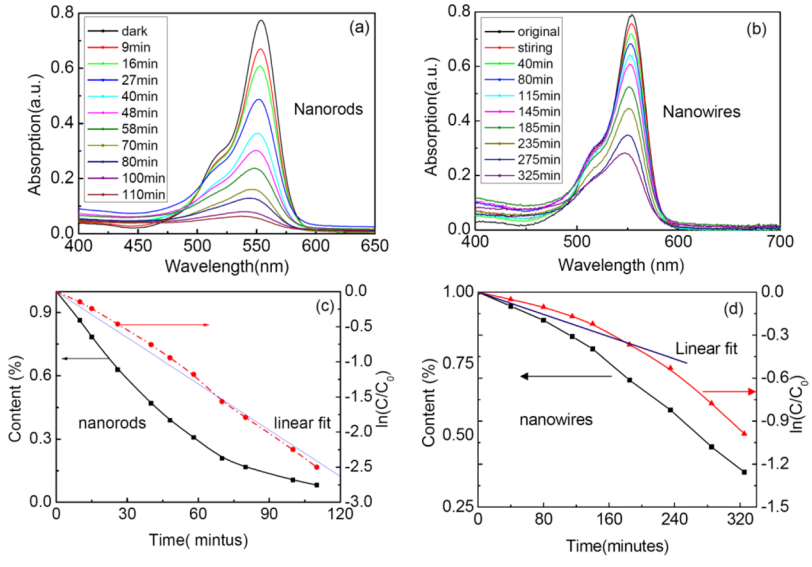

Figure 5. Absorption spectra of RhB dye solution with the $ZnWO_4$ nanorods (a) and nanowires (b) in different stages under illumination of the simulated sunlight; the content (%), $\ln(C/C_0)$ function and linear fit of $\ln(C/C_0)$ function of RhB vs reaction time by nanorods (c) and $ZnWO_4$ nanowires (d).

dx.doi.org/10.1021/am503696b | ACS Appl. Mater. Interfaces 2014, 6, 14423–14432

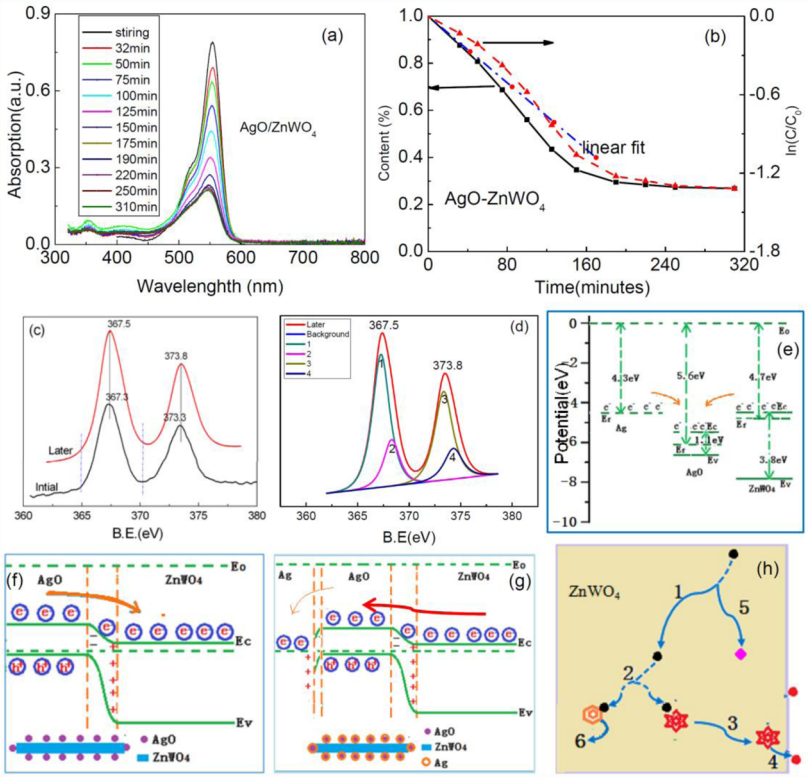

Figure 6. Photodegradation of RhB with the $AgO/ZnWO_4$ nanowires in different stages (a); the content (%), $\ln(C/C_0)$ function and linear fit of $\ln(C/C_0)$ function of RhB vs reaction time (b); the XPS spectra of the $AgO/ZnWO_4$: a typical survey spectrum of Ag core level at the initial (c) and later (d) degradation stages; the work function of individual Ag, AgO, $ZnWO_4$ (e); the photon-generated carrier diffusion (yellow arrows) and tunneling effect (red arrows) of $AgO/ZnWO_4$ (f) and $Ag/AgO/ZnWO_4$ (g). The example of photogenerated electron behaviors in $ZnWO_4$ during the degradation process (h). The red circle, purple diamond, orange hexagon, red sexangle and black circle present RhB, holes, WO_6 group, ZnO_6 group and photogenerated electrons, respectively. The excited electrons experience the following competitive processes: (1) transition from higher level to lower level, (2) trapped carrier's competition of WO_6 group and ZnO_6 group, (3) carrier's transition in ZnO_6 groups to surface, (4) bound electronic photodegradation RhB with the help of adsorbed oxygen in the surface, (5) nonradiative recombination and (6) radiative recombination.

vibration energy. So, $CoWO_4$ does not do very well in producing photocurrents and PL.

On the basis of DFT, charge injection or extraction and carrier transport of Co cation are weak, which agrees with the fluorescence quenching (Figure 3d) and weak photocurrent (Figure 3f). The strong cruise feature of the 4s states of the Zn cation in the ZnO_6 group makes large carrier transport and charge injection or extraction, which contributes to larger photoconduction and effectively increases photocatalytic performance. Such excited electrons and holes with high mobility contribute to the high photocatalytic performance, which is also observed in $PbWO_4$ with Pb^{2+} $5d^{10}$.[24] Therefore, high photocatalytic materials should not only have an active structure for direct electrons transition from the valence band to the conduction band without the help of phonons but also a special electronic configuration for the high mobility to ensure more excited electrons and holes in catalytic reaction. In addition, the activities of a material with electron states d^0, d^5 and d^{10} are lowest in most reactions, whereas that of d^7 and d^8 are high. That is to say, the ZnO_6 and WO_6 groups are stable in catalytic reactions and easily keep their catalytic activity, whereas the CoO_6 group can be liable to change valence, which lowers its catalytic performance.

In addition, a large surface area contributes to photocatalytic performance.[34] As are presented in Figure 5a,b, both 100 mg of $ZnWO_4$ nanorods and nanowires show good activity for the degradation of RhB aqueous solution (1×10^{-5} mol L^{-1}). From the plots of the content (%) vs the irradiation time (Figure 5c,d), the first-order kinetic constants of $k_1 = -0.021\,92$ min^{-1}, $k_2 = -0.001\,94$ min^{-1} for the $ZnWO_4$ nanorods and nanowires (a deviation from the straight line), respectively, are obtained by fitting linearly the first part of the plots, revealing an obvious lower activity of the nanowires than that of the nanorods. The first dynamics equation of the nanorods suggests a higher percentage of RhB adsorption on the surface of nanorods, and that the catalytic rate is decided by the amount of photogenerated electrons and holes, not by the initial concentration of the dye. It is well-known that a larger surface area has more surface defects, which absorb more dye to produce photon-generated carriers and the charge separation (effective suppression of the electron−hole recombination) under the irradiation. The ratio of surface to volume (RSV) can be defined as

$$\mathrm{RSV} = \frac{2\pi r^2 + 2\pi rL}{\pi r^2 L} \tag{7}$$

where, r and L are the radius and length of naorods, respectively. As the diameter of nanowires and nanorods are almost the same from the TEM, the RSV of nanowires and nanorods are 0.11/nm and 0.13/nm, respectively. The larger RSV of the nanorods means higher adsorptive capacity of RhB because the lager surface tends to lower its free energy by adsorption of free ions or molecule. In addition, the nanorods with smaller E_g can absorb more solar energy than that of

nanowires, which also contributes to higher photocatalytic performance. More excited carrier separation, larger adsorption capacity for dye on the surface and better light absorption contribute to a better photocatalytic performance.

It is an important method to improve photocatalytic performance by band modification. AgO with a band gap of about 1.1 eV has a strong absorption in the near-infrared and throughout the visible region.[42] The photodegradation of RhB under the simulated sunlight for different times in the presence of AgO/$ZnWO_4$ is shown in Figure 6a. The photodegradation is enhanced greatly in the initial stage. From the plot of the content (%) vs irradiation time (Figure 6b), straight lines can be linearly fitted with the first-order kinetic constants k_3 = −0.006 36 min^{-1}, which is much larger than k_2 = −0.001 94 min^{-1} for the $ZnWO_4$ nanowires. Almost 60% RhB can be effectively degraded within 150 min, whereas only 23% of the dye degraded (Figure 5b,d) with the $ZnWO_4$ nanowires in the same condition, but the ensuing photodegradation becomes difficult (the absorption spectrum intensity almost keeps constant).

To figure out the difference of photodegradation performance in the initial and later stages, the high-resolution X-ray photoelectron spectroscopy (XPS) spectra of Ag 3d for the AgO/$ZnWO_4$ before and after degradation of RhB for 300 min are shown in Figure 6c,d. The two samples were washed several times with deionized water and ethanol and then dried at 60 °C in air for 1 h before XPS measurement. The spectrum of the Ag exhibits two peaks at 367.3 and 373.3 eV in the initial sample, which is assigned to Ag $3d_{3/2}$ and Ag $3d_{5/2}$, respectively, corresponding to AgO.[43] However, the two peaks move to a little higher energy located in 367.5 and 373.8 eV, respectively, and widen, for the latter sample, which results in the Ag valence state change. To investigate the variation, the peaks at 367.5 and 373.8 eV are divided into 2 weeks, respectively, i.e., 367.3 eV (peak 1), 368.3 eV (peak 2) and 373.3 eV (peak 3), 374.3 eV (peak 4) as are shown in Figure 6d. Compared with other XPS data, we found that Ag element on the surface of $ZnWO_4$ nanowires is a mixture of AgO and metallic silver.[43] The results suggest that AgO nanoparticles are unstable under simulated sunlight irradiation and metallic Ag results from AgO reduction by electron oxidization action of conduction band of $ZnWO_4$. According to previous reports, AgO was thermally stable up to 373 K and completed thermal decomposition to Ag and O occurred at 673 K.[44] At the treatment temperature 60 °C in air, AgO is stable and the treatments would not induce AgO decomposition. Hence Ag detected by XPS is produced in the photocatalytic degradation RhB process. This is similar to the previous report that the Ag species are obtained from Ag_2O phase by electron reducing action of the conduction band of TiO_2 nanobelts under UV irradiation.[18] In addition, the Ag element contents before and after photodegradation were approximatly 5.75 and 6.57 at. %, respectively. The increase of Ag element contents may be ascribed to the decomposition of AgO producing oxygen, which decreases the total atoms of AgO/$ZnWO_4$.

To study the possible mechanism of high photocatalytic activity under simulated sunlight, the work function of bulk $ZnWO_4$, Ag and AgO of about 4.8, 4.3 and 5.6 eV[25,45] are shown in Figure 6e, and the schematic diagrams of the band configuration of AgO/$ZnWO_4$ and Ag/AgO/$ZnWO_4$ heterostructures are shown in Figure 6f,g. Because of the larger work function of AgO, the Fermi level of AgO is lower than that of $ZnWO_4$. When AgO contacts with $ZnWO_4$, the interface electrons flow from $ZnWO_4$ to AgO resulting in a built-in electric field directed from $ZnWO_4$ to AgO established at the same time, which can stop the charge diffusion. When the two semiconductors acquire an equalized Fermi level in the AgO/$ZnWO_4$ heterostructure, the conduction band minimum of AgO is higher than $ZnWO_4$, as is shown in Figure 6f. Under the simulated sunlight irradiation, the photogenerated electrons in the conduction band migrate from AgO to the conduction band of $ZnWO_4$, leaving the holes in the AgO valence band. In the present study, the photocurrent in Figure 3c reveals that the efficiencies of the charge migration and transfer are higher in $ZnWO_4$ before photogenerated carrier recombination under the applied bias. Usually, the electronic mobility is greater than that of the hole (about 3 times), which results in abundant electrons concentrating on $ZnWO_4$ and a lot of holes in AgO. So, the heterostructure can greatly enhance the separation of electron−hole pairs, resulting in the enhancement of photocatalytic actives. These energetic states can activate many chemical reactions at the semiconductors' surface. The excitation electron behaviors in $ZnWO_4$ are presented in Figure 6h.

AgO is generally considered as the existence of Ag^{1+} and Ag^{3+} configurations due to a small on-site Coulomb interaction, U_{dd}.[44] Ag^{3+} has the strong ability of trapping electrons. When under simulated sunlight irradiation, Ag^{3+} can act as produced electron traps.[44,46,47] Simultaneously, when fine particles of transition metals or their oxides are dispersed on the surface of a photocatalyst matrix, transition metals or their oxides can act as electron traps on *n*-type semiconductors.[46,47] Because the diameter of AgO particles is about 5 nm, quantum tunneling is very significant. Electrons transmission from $ZnWO_4$ to AgO nanoparticles overcome the built-in electric field are effective and some electrons are continuously trapped by Ag^{3+} to form Ag, consistent with the existence of Ag element detected by the XPS spectra (Figure 6c,d).

As the experiment progressed, metallic Ag nanoparticles are generated and aggregated on the surface of AgO, forming the Ag/AgO/$ZnWO_4$ heterostructure. Based on the strong local field of noble metals, strong interaction exists between metallic Ag nanoparticles and rhodamine B, suggesting that RhB in solution quickly decreases after the high adsorption of RhB by Ag nanoparticles. Through combination of the adsorption of RhB by Ag nanoparticles and degradation of RhB by $ZnWO_4$, the RhB concentration decreases rapidly in the first 150 min. However, the photocatalytic activity of AgO/$ZnWO_4$ heterostructure continuously decreases after 150 min.

For further explanation, the change of photocatalytic activity, the band structure and charge separation at the interface of Ag/AgO/$ZnWO_4$ is shown in Figure 6g. Because of the bigger work function of AgO shown in Figure 6e, the Fermi level of AgO is lower than that of Ag. When AgO contacts with Ag, the electrons flow from Ag to AgO and holes flow from AgO to Ag, resulting in a built-in electric field from Ag to AgO at the same time, which can stop the charge diffusion.[45] The two phases acquire an equalized Fermi level, and the energy band of Ag shifts downward along with its Fermi level in the process. Under the simulated sunlight irradiation, only $ZnWO_4$ nanowires absorb sunlight because AgO is coated by Ag, which does not absorb sunlight (except plasma resonance). So, the effective light absorption of the Ag/AgO/$ZnWO_4$ obviously decreases due to the blocking sunlight by metallic Ag. Because the conduction band potential of AgO is higher than that of Ag, the photogenerated electrons are beneficial to migrate from

AgO to Ag and the electrons in CB of $ZnWO_4$ migrate to AgO nanoparticles based on the quantum tunnelling effect. Therefore, the photogenerated electrons and holes involving in the photocatalytic reaction decrease and the photocatalytic reaction has been suppressed. Finally, the effective adsorption of RhB by $ZnWO_4$ decreases because of the strong adsorption of RhB by Ag nanoparticles. Consequently, the effective photocatalytic reaction on the $ZnWO_4$ surface is reduced greatly in the final stage.

It is hard to believe that complete silver ion reduction occurs on the surface of AgO/$ZnWO_4$. Ershov proposed that the great efficiency of complete silver reduction is due to the exceptionally high specific rate of the reaction of e_{aq-} (mainly obtained from AgO) with Ag^+; thus, this reaction can successfully compete with the reactions of the hydrated electron with itself and with the carboxyl radical anion (CO_2^-, which comes from the photodegradation fragments).[48] Therefore, the large silver particles formed tend to agglomerate rapidly. It is well-known that the number of absorption peaks usually increases as the symmetry of nanoparticles is decreased: spherical nanoparticles (with *Cs* symmetry) exhibit only one peak. The absorption spectrum of spherical silver nanoparticles with a mean diameter of 5.6 ± 3.9 nm has a peak at 391 nm and an absorption valley at about 320 nm. As the size of silver increases, the absorption peaks are red-shifted.[49] Figure 7 presents the absorption spectrum of AgO/$ZnWO_4$ after degradation of RhB for 4 h. Absorption peaks at about 380 and 490 nm correspond to absorption peaks of Ag and AgO. And the absorption valley at about 320 nm is found. The absorption spectrum indicates Ag nanoparitals aggregate on the surface of AgO/$ZnWO_4$ and the aggregates are spherical nanoparticles with a mean diameter of less than 5.6 nm. The BET surface area, pore size and pore volume of the AgO/$ZnWO_4$ after degradation are 20.67 m^2/g, 23.87 nm, 0.12 cm^3/g for 0 h, 20.80 m^2/g, 24.03 nm, 0.13 cm^3/g for 2 h and 21.05 m^2/g, 23.76 nm, 0.11 cm^3/g for 4 h, respectively. Therefore, precipitated silver attached to the surface of the AgO/$ZnWO_4$ increases the surface areas. The excess Ag aggregates lead to pore blocking and decrease the pore volumes. Therefore, activity of the AgO/$ZnWO_4$ decreases. The experimental results are consistent with the theoretical hypothesis on the band structure.

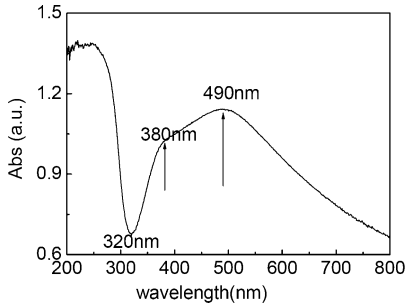

Figure 7. Absorption spectrum of the AgO/$ZnWO_4$ after photodegradation of RhB for 4 h.

It has been reported that the mechanism of mineralization includes two competitive processes: a photocatalytic process and a photosensitized process.[50] However, the photosensitized process does not exist in some photodegradation because the excited electrons in some dye cannot transfer to the photocatalyst conduction band due to the fact that the level of dye excited states is lower than that of the photocatalyst conduction band. To explore the photocatalytic activity in other organic contaminations and the role of the photosensitized process on photodegradation, the photodegradation of 100 mL (1.2×10^{-5} mol·L^{-1}) of RhB with 100 mg of $ZnWO_4$ nanowires under monochromatic light (546 nm) irradiation is conducted because the absorption of RhB on the monochromatic light (at 553 nm) is 86.7% of the maximum absorption strength. Figure 8a presents the absorption spectrum of different time photodegradations of RhB with $ZnWO_4$ nanowires. Only 4% of the dye is degraded within 184 min and $k_4 = -0.0002$ min^{-1}, which is much smaller than $k_2 = -0.001\,94$ min^{-1} shown in Figure 8b. Therefore, the photosensitized process would be neglected.

CONCLUSIONS

The photocatalytic performance of $ZnWO_4$ is systematically studied by investigating its band structure, morphology and surface modification. The experimental results indicate that the photocatalytic activity of ZnWO is greater than that of $CoWO_4$ for the itinerant electron Zn 4s in the ZnO_6 group. Compared with $ZnWO_4$ nanowires, $ZnWO_4$ nanorods exhibit better photocatalytic activity for its larger surface area, which contributes to the effective optical absorption, higher density catalytic active sites, better adsorption of RhB on the surface and lower rate of recombination of holes and electrons (Figure 8). The photocatalytic activity of AgO-loaded $ZnWO_4$ is greatly enhanced when compared with pure $ZnWO_4$ nanowires at the initial stage for the efficient separation of electron−hole pairs and prevention of the recombination of electron−hole pairs. However, AgO nanorods are slowly deoxidized and form a multiphase heterostructure of Ag/AgO/$ZnWO_4$, which reduces

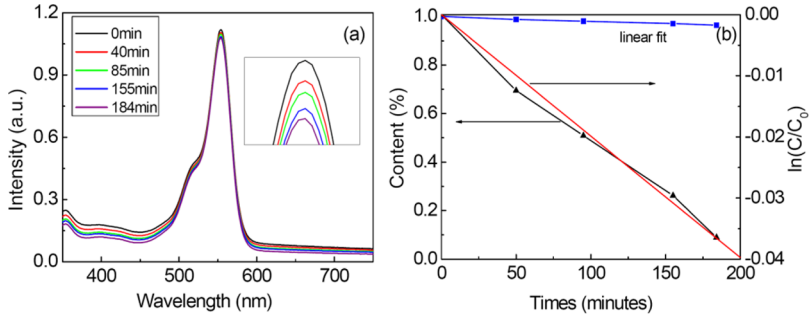

Figure 8. Absorption spectrum (a) and partially enlarged curves (inset a) of RhB dye solution with the $ZnWO_4$ nanorods in different stages under illumination at about 546 nm; the content (%), $\ln(C/C_0)$ function and linear fit of $\ln(C/C_0)$ function of RhB vs reaction time of $ZnWO_4$ nanowires (b).

photocatalytic activity, owing to the reduction of effective optical absorption, the block of adsorption of RhB on the $ZnWO_4$ surface and the reduction of electron−hole pairs' separation. Anyhow, a little photosensitized degradation of RhB is found in the process. Hence, the trapped carrier's competition of the WO_6 group and ZnO_6 group, recombination, carrier's transition, adsorbed RhB and adsorbed oxygen in the surface have an enormous influence on the ability of light degradation. On the basis of our investigations, high photocatalytic materials should not only have active structures for direct electron transitions from the valence band to the conduction band without the help of phonons but also a special electronic configuration for the high mobility to ensure more excited electrons and holes participating in catalytic reactions. This investigation contributes to the fabrication of a better efficient photocatalyst for the elimination of environmental pollutants.

AUTHOR INFORMATION

Corresponding Author

*C. Hu. E-mail: hucg@cqu.edu.cn. Tel: +86 23 65678362. Fax: +86 23 65678362.

Notes

The authors declare no competing financial interest.

ACKNOWLEDGMENTS

This work is supported by the Science and Technology Research Project of Chongqing Municipal Education Commission of China (KJ1400607), the NSFCQ (cstc2012jjB0006), SRFDP (20110191110034, 20120191120039), NSFC (11204388)

REFERENCES

(1) Fujishima, A.; Zhang, X. T.; Tryk, D. A. TiO_2 Photocatalysis and Related Surface Phenomena. *Surf. Sci. Rep* **2008**, *63*, 515−582.

(2) Zhang, Z. B.; Wang, C. C.; Zakaria, R. Role of Particle Size in Nanocrystalline TiO_2-based Photocatalysts. *J. Phys. Chem. B* **1998**, *102*, 10871−10878.

(3) Liu, G.; Wang, L. Z.; Yang, H. G. Titania-based Photocatalysts-Crystal Growth, Doping and Heterostructuring. *J. Mater. Chem.* **2010**, *20*, 831−843.

(4) Yu, J. G.; Wang, G. H.; Cheng, B. Effects of Hydrothermal Temperature and Time on the Photocatalytic Activity and Microstructures of Bimodal Mesoporous TiO_2 Powders. *Appl. Catal., B* **2007**, *69*, 171−180.

(5) Wu, N. Q.; Wang, J.; Tafen, D. Nyago; Shape-Enhanced Photocatalytic Activity of Single-Crystalline Anatase TiO_2 (101) Nanobelts. *J. Am. Chem. Soc.* **2010**, *132*, 6679−6685.

(6) Xu, A. W.; Gao, Y.; Liu, H. Q. The Preparation, Characterization, and Their Photocatalytic Activities of Rare-Earth-Doped TiO_2 Nanoparticles. *J. Catal.* **2002**, *207*, 151−157.

(7) Choi, W. Y.; Termin, A.; Hoffmann, M. R. The Role of Metal-Ion Dopants in Quantum-sized TiO_2 - Correlation Between Photoreactivity and Charge-Carrier Recombination Dyamics. *J. Phys. Chem.* **1994**, *98*, 13669−13679.

(8) Zheng, Y. H.; Chen, C. Q.; Zhan, Y. Y. Photocatalytic Activity of Ag/ZnO Heterostructure Nanocatalyst: Correlation between Structure and Property. *J. Phys. Chem. C* **2008**, *112*, 10773−10777.

(9) Ullah, R.; Dutta, J. Photocatalytic Degradation of Organic Dyes with Manganese-Doped ZnO Nanoparticles. *J. Hazard. Mater.* **2008**, *156*, 194−200.

(10) Wang, J.; Qu, F. Y.; Wu, X. Photocatalytic Degradation of Organic Dyes with Hierarchical Ag_2O/ZnO Heterostructures. *Sci. Adv. Mater.* **2013**, *5*, 1364−1371.

(11) He, X. Y.; Hu, C. G.; Yi, Q. N.; Wang, X.; Hua, Hao.; Li, X. Y. Preparation and Improved Photocatalytic Activity of WO_3-$0.33H_2O$ Nanonetworks. *Catal. Lett.* **2012**, *142*, 637−645.

(12) Amano, F.; Nogami, K.; Ohtani, B. Visible Light-Responsive Bismuth Tungstate Photocatalysts: Effects of Hierarchical Architecture on Photocatalytic Activity. *J. Phys. Chem. C* **2009**, *113*, 536−1542.

(13) Xu, J.; Hu, C. G.; Liu, G. B.; Liu, H.; Du, G. J.; Zhang, Y. Synthesis and Visible-Light Photocatalytic Activity of $NdVO_4$ Nanowires. *J. Alloys Compd.* **2011**, *509*, 7968−7972.

(14) Asahi, R.; Morikawa, T.; Ohwaki, T. Visible-Light Photocatalysis in Nitrogen-Doped Titanium Oxides. *Science* **2001**, *293*, 269−271.

(15) Sridharan, K.; Park, T. J. Thorn-Ball Shaped TiO2 Nanostructures: Influence of Sn^{2+} Doping on the Morphology and Enhanced Visible Light Photocatalytic Activity. *Appl. Catal., B* **2013**, *134*, 174−184.

(16) Zheng, J. Y.; Yu, H.; Li, X. J.; Zhang, S. Q. Enhanced Photocatalytic Activity of TiO_2 Nano-structured Thin Film with a Silver Hierarchical Configuration. *Appl. Surf. Sci.* **2008**, *254*, 1630−1635.

(17) Kohtani, S.; Hiro, J.; Yamamoto, N.; Kudo, A.; Tokumura, K.; Nakagaki, R. Adsorptive and Photocatalytic Properties of Ag-loaded $BiVO_4$ on the Degradation of 4-n-alkylphenols under Visible Light Irradiation. *Catal. Commun.* **2005**, *6*, 185−189.

(18) Zhou, W.; Liu, H.; Wang, J.; Liu, D.; Du, G.; Cui, J. Ag_2O/TiO_2 Nanobelts Heterostructure with Enhanced Ultraviolet and Visible Photocatalytic Activity. *ACS Appl. Mater. Interfaces.* **2010**, *8*, 2385−2392.

(19) Hashim, M.; Hu, C. G.; Wang, X.; Wan, B. Y.; Xu, J. Room Temperature Synthesis and Photocatalytic Property of AgO/$Ag_2Mo_2O_7$ Heterojunction Nanowires. *Mater. Res. Bull.* **2012**, *47*, 3383−3389.

(20) Saito, N.; Matsumoto, H.; Kobayashi, H.; Ikarashi, K.; Nishiyama, H.; Inoue, Y. A New Photocatalyst of RuO_2-loaded $PbWO_4$ for Overall Splitting of Water. *Chem. Lett.* **2004**, *133*, 1452−1453.

(21) Montini, T.; Gombac, V.; Hameed, A.; Felisari, L.; Adami, G.; Fornasiero, P. Synthesis, Characterization and Photocatalytic Performance of Transition Metal Tungstates. *Chem. Phys. Lett.* **2010**, *498*, 113−119.

(22) Fu, H. B.; Pan, C. S.; Zhang, L. W.; Zhu, Y. F. Synthesis, Characterization and Photocatalytic Properties of Nanosized Bi_2WO_6, $PbWO_4$ and $ZnWO_4$ Catalysts. *Mater. Res. Bull.* **2007**, *42*, 696−706.

(23) Fu, H. B.; Zhang, L. W.; Yao, W. Q.; Zhu, Y. F. Photocatalytic Properties of Nanosized Bi_2WO_6 Catalysts Synthesized via a Hydrothermal Process. *Appl. Catal., B* **2006**, *66*, 100−110.

(24) Haruhiko, K.; Nobuo, S.; Hiroshi, N.; Hisayoshi, K.; Yoshiki, S.; Yasunobu, I. Overall Splitting of Water by RuO_2-loaded $PbWO_4$ Photocatalyst with $d^{10}s^2$-d^0 Configuration. *J. Phys. Chem. C* **2007**, *111*, 439−444.

(25) Perales, R. L.; Fuertes, J. R.; Errandonea, D.; García, D. M.; Segura, A. Optical Absorption of Divalent Metal Tungstates: Correlation between the Band-Gap Energy and the Cation Ionic Radius. *Europhys. Lett.* **2008**, *83*, 37002−37018.

(26) Huang, G. L.; Zhang, C.; Zhu, Y. F. $ZnWO_4$ Photocatalyst with High Activity for Degradation of Organic Contaminants. *J. Alloys Compd.* **2007**, *432*, 269−276.

(27) Yan, T. J.; Li, L. P.; Tong, W. M.; Zheng, J.; Wang, Y. J.; Li, G. S. $CdWO_4$ Polymorphs: Selective Preparation, Electronic Structures, and Photocatalytic Activities. *J. Solid State Chem.* **2011**, *184*, 357−364.

(28) Fu, H. B.; Pan, C. S.; Zhang, L. W.; Zhu, Y. F. Synthesis, Characterization and Photocatalytic Properties of Nanosized Bi_2WO_6, $PbWO_4$ and $ZnWO_4$ Catalysts. *Mater. Res. Bull.* **2007**, *42*, 696−706.

(29) *Aquatic Chemistry: Interfacial and Interspecies Processes*; Huang, C. P.; O'Melia, C. R.; Morgan, J. J., Eds.; Advances in Chemistry Series 244; American Chemical Society, Washington, DC, 1995.

(30) Dai, X. J.; Luo, Y. S.; Zhang, W. D.; Fu, S. Y. Facile Hydrothermal Synthesis and Photocatalytic Activity of Bismuth Tungstate Hierarchical Hollow Spheres with an Ultrahigh Surface Area. *Dalton Trans.* **2010**, *39*, 3426−3432.

(31) Wang, J.; Tafen, D. N.; Lewis, J. P.; Hong, Z. L.; Manivannan, A.; Zhi, M. J.; Li, M.; Wu, N. Q. Origin of Photocatalytic Activity of Nitrogen-doped TiO_2 Nanobelts. *J. Am. Chem. Soc.* **2009**, *131*, 12290−12297.
(32) Wang, D. J.; Xue, G. L.; Zhen, Y. Z.; Feng, F.; Li, D. S. Monodispersed Ag Nanoparticles Loaded on the Surface of Spherical Bi_2WO_6 Nanoarchitectures with Enhanced Photocatalytic Activities. *J. Mater. Chem.* **2012**, *22*, 4751−4758.
(33) Li, D.; Shi, R.; Pan, C. S.; Zhu, Y. F.; Zhao, H. J. Influence of $ZnWO_4$ Nanorod Aspect Ratio on the Photocatalytic Activity. *CrystEngComm* **2011**, *13*, 4695−4700.
(34) Huang, G. L.; Zhu, Y. F. Synthesis and Photocatalytic Performance of $ZnWO_4$ Catalyst. *Cryst. Eng. Comm* **2012**, *14*, 8076−8082.
(35) Singh, P.; Raizada, P.; Pathania, D.; Kumar, A.; Thakur, P. Preparation of BSA-$ZnWO_4$ Nanocomposites with Enhanced Adsorptional Photocatalytic Activity for Methylene Blue Degradation. *Int. J. Photoenergy* **2013**, *2013*, 1−7.
(36) Sun, L. M.; Zhao, X.; Jia, C. J.; Zhou, X. Y.; Cheng, X. F.; Li, P.; Liu, L.; Fan, W. L. Enhanced Visible-Light Photocatalytic Activity of g-C_3N_4−$ZnWO_4$ by Fabricating a Heterojunction: Investigation Based on Experimental and Theoretical Studies. *J. Mater. Chem.* **2012**, *22*, 23428−23438.
(37) Aysin, B.; Ozturk, A.; Park, J. Silver-loaded TiO_2 Powders Prepared through Mechanical Ball Milling. *Ceram. Int.* **2013**, *39*, 7119−7126.
(38) Wang, X. F.; Li, S. F.; Yu, H. G.; Yu, J. G.; Liu, S. W. Ag_2O as a New Visible-Light Photocatalyst: Self-Stability and High Photocatalytic Activity. *Chem.—Eur. J.* **2011**, *17*, 7777−7780.
(39) Errandonea, D.; Pellicer-Porres, J.; Manjón, F. J.; Segura, A. High-Pressure Structural Study of the Scheelite Tungstates $CaWO_4$ and $SrWO_4$. *Phys. Rev. B* **2005**, *72*, 174106−174158.
(40) Li, X. Y.; Hu, C. G.; Wang, X.; Xi, Y. Photocatalytic Activity of CdS Nanoparticles Synthesized by a Facile Composite Molten Salt Method. *Appl. Surf. Sci.* **2012**, *258*, 4370−4376.
(41) Li, X. Y.; Xi, Y.; Hu, C. G.; Wang, X. Water Induced Size and Structure Phase Transition of CdS Crystals and their Photocatalytic Property. *Mater. Res. Bull.* **2013**, *48*, 295−299.
(42) Feng, H. L.; Gao, X. Y.; Zhang, Z. Y.; Ma, J. M. Study on the Crystalline Structure and the Thermal Stability of Silver-Oxide Films Deposited by Using Direct-Current Reactive Magnetron Sputtering Methods. *J. Korean Phys. Soc.* **2010**, *56*, 1176−1179.
(43) Hoflund, G. B.; Hazos, Z. F. Surface Characterization Study of Ag, AgO, and Ag_2O Using X-ray Photoelectron Spectroscopy and Electron Energy-Loss Spectroscopy. *Phys. Rev. B* **2000**, *62*, 11125−11133.
(44) Waterhouse, G. I. N.; Bowmaker, G. A.; Metson, J. B. The Thermal Decomposition of Silver (I, III) Oxide: A Combined XRD, FT-IR and Raman Spectroscopic Study. *Phys. Chem. Chem. Phys.* **2001**, *3*, 3838−3845.
(45) Li, P.; Zhao, X.; Jia, C. J.; Sun, H. G.; Sun, L. M.; Cheng, X. F.; Li, L. B.; Fan, W. L. $ZnWO_4$/BiOI Heterostructures with Highly Efficient Visible Light Photocatalytic Activity: The Case of Interface Lattice and Energy Level Match. *J. Mater. Chem. A* **2013**, *1*, 3421−3429.
(46) Li, Q.; Xie, R. C.; Mintz, E. A.; Shang, J. K. Enhanced Visible-Light Photocatalytic Degradation of Humic Acid by Palladium Oxide-sensitized Nitrogen-Doped Titanium Oxide. *J. Am. Ceram. Soc.* **2007**, *90*, 3863−3868.
(47) Subramanian, V.; Wolf, E.; Kamat, P. V. To What Extent Metal Nanoparticles (Au, Pt, Ir) Improve the Photocatalytic Activity of TiO_2 films? *J. Phys. Chem. B* **2001**, *105*, 11439−11446.
(48) Ershov, B. G.; Janata, E.; Henglein, A.; Fojtik, A. Silver Atoms and Clusters in Aqueous Solution: Absorption Spectra and the Particle Growth in the Absence of Stabilizing Ag^+ Ions. *J. Phys. Chem.* **1993**, *97*, 4589−4594.
(49) Sun, Y. G.; Xia, Y. N. Gold and Silver Nanoparticles: A Class of Chromophores with Colors Tunable in the Range from 400 to 750 nm. *Analyst* **2003**, *128*, 686−691.
(50) Bunsho, O. Preparing Articles on Photocatalysis—Beyond the Illusions, Misconceptions, and Speculation. *Chem. Lett.* **2008**, *37*, 217−229.